The auxiliary subunit γ_1 of the skeletal muscle L-type Ca^{2+} channel is an endogenous Ca^{2+} antagonist

Zoita Andronache*, Daniel Ursu*, Simone Lehnert†, Marc Freichel†, Veit Flockerzi†, and Werner Melzer*‡

*Institut für Angewandte Physiologie, Universität Ulm, Albert-Einstein-Allee 11, D-89069 Ulm, Germany; and †Institut für Pharmakologie und Toxikologie, Universität des Saarlandes, D-66421 Homburg, Germany

Edited by Clara Franzini-Armstrong, University of Pennsylvania School of Medicine, Philadelphia, PA, and approved August 29, 2007 (received for review May 14, 2007)

Ca^{2+} channels play crucial roles in cellular signal transduction and are important targets of pharmacological agents. They are also associated with auxiliary subunits exhibiting functions that are still incompletely resolved. Skeletal muscle L-type Ca^{2+} channels (dihydropyridine receptors, DHPRs) are specialized for the remote voltage control of type 1 ryanodine receptors (RyR1) to release stored Ca^{2+}. The skeletal muscle-specific γ subunit of the DHPR (γ_1) down-modulates availability by altering its steady state voltage dependence. The effect resembles the action of certain Ca^{2+} antagonistic drugs that are thought to stabilize inactivated states of the DHPR. In the present study we investigated the cross influence of γ_1 and Ca^{2+} antagonists by using wild-type ($\gamma+/+$) and γ_1 knockout ($\gamma-/-$) mice. We studied voltage-dependent gating of both L-type Ca^{2+} current and Ca^{2+} release and the allosteric modulation of drug binding. We found that 10 μM diltiazem, a benzothiazepine drug, more than compensated for the reduction in high-affinity binding of the dihydropyridine agent isradipine caused by γ_1 elimination; 5 μM devapamil [(−)D888], a phenylalkylamine Ca^{2+} antagonist, approximately reversed the right-shifted voltage dependence of availability and the accelerated recovery kinetics of Ca^{2+} current and Ca^{2+} release. Moreover, the presence of γ_1 altered the effect of D888 on availability and strongly enhanced its impact on recovery kinetics demonstrating that γ_1 and the drug do not act independently of each other. We propose that the γ_1 subunit of the DHPR functions as an endogenous Ca^{2+} antagonist whose task may be to minimize Ca^{2+} entry and Ca^{2+} release under stress-induced conditions favoring plasmalemma depolarization.

accessory subunits | dihydropyridine receptor | excitation–contraction coupling | mouse skeletal muscle | phenylalkylamine

Owing to the central role of Ca^{2+} channels in cellular signaling, Ca^{2+} channel modulators have become important pharmacological tools in research and clinical applications. Prominent examples are Ca^{2+} antagonists (Ca^{2+} entry blockers) used to target muscle cells of the cardiovascular system in the treatment of hypertension, angina pectoris, and cardiac arrhythmias (1, 2). In skeletal muscle, the dihydropyridine receptor (DHPR), an L-type Ca^{2+} channel, plays a pivotal role as a voltage sensor for the remote control of type 1 ryanodine receptors (RyR1). Through a unique conformational link, the voltage-sensing α_1 subunit of the DHPR ($Ca_v1.1$) activates RyR1 to rapidly mobilize Ca^{2+} stored in the terminal cisternae of the sarcoplasmic reticulum (SR) for the initiation of contraction. It is not clear yet whether the same DHPRs that control Ca^{2+} release also generate the slow L-type Ca^{2+} current that can be observed in skeletal muscle. In any case, a Ca^{2+} inward current is not required as a trigger for Ca^{2+} release in contrast to heart muscle. Yet, the DHPR-dependent control mechanism of release is affected by Ca^{2+} antagonists (for review, see ref. 3). Depolarizing the membrane of isolated frog fibers by applying a high-potassium solution containing the phenylalkylamine (PAA) Ca^{2+} channel antagonist D600 (30 μM) was shown to cause a normal contracture followed by paralysis (4). By using voltage-clamp conditions, it could be demonstrated that the paralysis by D600 or by the higher-affinity PAA drug D888 was removed by hyperpolarizing the fiber membrane to potentials between −120 and −150 mV (5, 6). These experiments revealed that the PAA-induced inhibition results from a concentration-dependent shift to more negative potentials of the steady-state voltage dependence of force availability, probably caused by a selective binding of the drug to the inactivated conformational state of the voltage sensor for Ca^{2+} release (5, 7, 8).

Voltage-dependent channels are hetero-oligomeric proteins containing several auxiliary subunits in addition to the pore-forming α-subunits (9). Ca^{2+} channels can be associated with up to four nonhomologous auxiliary subunits named α_2, β, γ, and δ, whose functional roles are still incompletely understood (10, 11). In the skeletal muscle L-type channel, the γ-subunit (γ_1), shows the highest tissue specificity next to the α_1-polypeptide. Interestingly, γ_1 deficiency in voltage-clamped adult muscle fibers of gene-targeted knockout mice affected both Ca^{2+} current and Ca^{2+} release by shifting the steady-state availability curves to more positive potentials (12). Thus, the γ_1-polypeptide exhibits a physiological effect similar to the one reported for PAA Ca^{2+} channel antagonists.

In this study we examined whether there is a connection between the Ca^{2+} antagonist- and the γ_1-induced functional changes. For this purpose, we studied the effect of D888 on Ca^{2+} current and Ca^{2+} release in isolated muscle fibers of both $\gamma+/+$ and $\gamma-/-$ mice. We report that an appropriate concentration of D888 can compensate for the effect of eliminating the γ_1-subunit, underlining the close similarity in the actions of PAA drugs and γ_1. We also show that the presence of γ_1 alters the pattern of action of D888. Moreover, we demonstrate that diltiazem, a benzothiazepine Ca^{2+} antagonist, can compensate for changes in dihydropyridine binding caused by the γ_1-subunit knockout. We propose that the Ca^{2+} antagonists and the subunit act by a closely connected physiological mechanism.

Results

D888 Does Not Affect Voltage-Dependent Activation. Fig. 1 shows the protocol to study voltage-dependent activation of L-type Ca^{2+} current and Ca^{2+} release in an enzymatically isolated interosseus muscle fiber of a $\gamma-/-$ mouse. Test steps of 100-ms duration, separated by intervals of 60 s, were applied covering the voltage range from −60 to +50 mV in 10-mV increments (Fig. 1*A*). Fig. 1*B* shows the Ca^{2+} inward current and Fig. 1*E* shows the corresponding current–voltage relation. Fig. 1*C* shows

Author contributions: Z.A., D.U., V.F., and W.M. designed research; Z.A. and S.L. performed research; M.F. and V.F. contributed new reagents/analytic tools; Z.A., D.U., S.L., V.F., and W.M. analyzed data; and Z.A. and W.M. wrote the paper.

The authors declare no conflict of interest.

This article is a PNAS Direct Submission.

Abbreviations: DHP, dihydropyridine; DHPR, dihydropyridine receptor; EC, excitation-contraction; PAA, phenylalkylamine; SR, sarcoplasmic reticulum.

‡To whom correspondence should be addressed. E-mail: werner.melzer@uni-ulm.de.

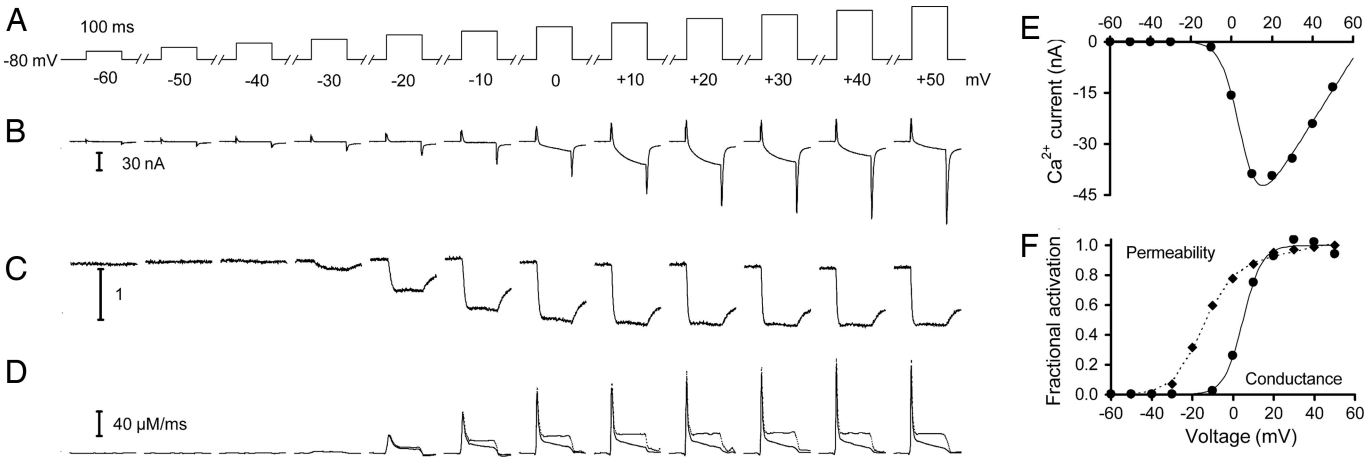

Fig. 1. Voltage-dependent activation of Ca^{2+} current and Ca^{2+} release. (*A*) Successive rectangular voltage steps applied at 60-s intervals from a holding potential of −80 mV to the indicated voltage levels. (*B*) Voltage-activated L-type Ca^{2+} inward currents showing typical slow-onset kinetics. (*C*) Fura-2 fluorescence ratio signals recorded simultaneously with the signals in *B*. (*D*) Calculated flux of Ca^{2+} underlying the signals in *C* before and after correction for putative SR depletion (see *Materials and Methods*). Traces for pulse voltages between 0 and +50 mV were corrected individually. For pulse voltages of −10 mV and smaller the average value of the individually determined baseline SR contents was used for the correction (see ref. 13). (*E*) Current–voltage relation derived from the recordings in *B*. (*F*) Ca^{2+} conductance (circles) and SR Ca^{2+} permeability (diamonds) during the plateau of the depletion-corrected signals in *D* as functions of pulse voltage. Representative data were obtained from a $\gamma-/-$ muscle fiber.

the fura-2 fluorescence ratio signals (F_{380}/F_{360}) and Fig. 1*D* shows the Ca^{2+} release flux derived from them. Ca^{2+} release flux was calculated as described in detail by Ursu *et al.* (13) after characterizing Ca^{2+} removal by using a kinetic model to fit relaxation following repolarization (see also refs. 14 and 15). The flux traces exhibit a slowly sloping phase after the early peak that had been attributed to SR depletion (16). We performed a depletion correction as described by Gonzalez and Ríos (17), leading to the second set of traces in Fig. 1*D* exhibiting steady plateaus. The depletion-corrected flux is proportional to the voltage-activated Ca^{2+} permeability of the SR. Fig. 1*F* shows fractional activation as functions of voltage both for permeability and for Ca^{2+} conductance derived from the current–voltage relation (13).

Fig. 2 summarizes the results of experiments testing for D888 effects on the voltage dependence of activation of L-type Ca^{2+} conductance and of SR permeability obtained with the protocol of Fig. 1. A comparison for 0 μm (circles) and 10 μM D888 (diamonds) is shown. Open symbols represent $\gamma-/-$ fibers and filled symbols indicate $\gamma+/+$. The data confirm our previous finding that γ_1 does not affect the voltage dependence of activation of Ca^{2+} release and L-type Ca^{2+} conductance. They further demonstrate that D888 at 10 μM, that is, at a higher concentration than leading to paralysis in frog muscle, has negligible effects on the activation curves both in the absence and the presence of γ_1. The absolute values of conductance and peak permeability are listed in the legend of Fig. 2. The mean values are slightly smaller in D888, but the difference is not statistically significant.

D888 Effect on Voltage-Dependent Inactivation. Whereas the voltage dependence of activation for both Ca^{2+} permeability and L-type Ca^{2+} conductance remained unaffected by the γ_1-subunit and by D888 (Fig. 2), pronounced effects were seen on inactivation. Fig. 3*A* shows the experimental paradigm to determine the voltage dependence of availability for activation. Prepulses of 30-s duration changing the membrane potential to progressively more depolarized values were followed by short (100 ms) test pulses to +20 mV to assess availability. Fig. 3 *B–E* show traces of two representative experiments in γ_1-deficient muscle fibers, demonstrating the effect of 5 μM D888 on availability of Ca^{2+} release flux (Fig. 3 *D* vs. *B*) and of L-type Ca^{2+} inward current (Fig. 3 *E* vs. *C*). Fig. 3 *F* and *G* show the alterations in the voltage dependence of steady-state inactivation caused by the drug for (peak) Ca^{2+} release and Ca^{2+} current, respectively. Clearly, a shift to more negative potentials by some 10 mV is apparent in both cases.

Fig. 4 summarizes the data obtained from several experiments like those shown in Fig. 3 performed on muscle fibers of $\gamma-/-$ mice (Fig.4 A and *B*) and $\gamma+/+$ animals (Fig. 4 *C* and *D*).

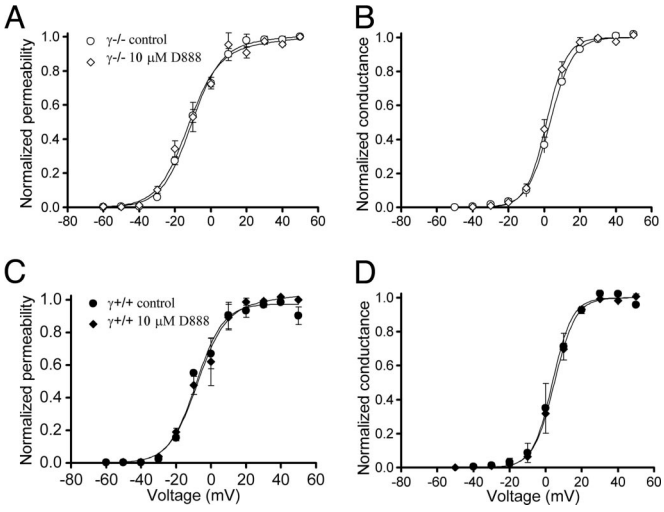

Fig. 2. Voltage-dependent activation independent of D888. Normalized activation curves for Ca^{2+} release permeability and conductance as in Fig. 1*F* for 0 μm (circles) and 10 μM D888 (diamonds). $V_{0.5}$ and *k* values (in millivolts) for control and drug application are as follows: (*A*) Permeability, $\gamma-/-$, -11.23 ± 1.90; 8.2 ± 0.52 (6) and -13.26 ± 2.92; 8.50 ± 0.7 (3). (*B*) Conductance, $\gamma-/-$, 3.2 ± 0.95; 6.3 ± 0.73 (6) and 1.22 ± 0.97; 5.62 ± 0.3 (3). (*C*) Permeability, $\gamma+/+$, -8.46 ± 1.40; 7.80 ± 0.93 (3) and -8.24 ± 1.70; 8.10 ± 0.5 (8). (*D*) Conductance, $\gamma+/+$, 3.71 ± 3.20; 5.44 ± 0.61 (3) and 4.81 ± 0.84; 5.83 ± 0.4 (6). The corresponding absolute values at +50 mV for peak permeability or conductance are: (*A*) $5.73 \pm 0.98\%ms^{-1}$ and $3.55 \pm 0.20\%ms^{-1}$. (*B*) 180.34 ± 38.17 S F^{-1} and 133.59 ± 14.13 S F^{-1}. (*C*) $5.39 \pm 1.51\%ms^{-1}$ and $3.82 \pm 0.45\%ms^{-1}$. (*D*) 109.09 ± 29.66 S F^{-1} and 92.13 ± 8.20 S F^{-1}. The continuous lines were calculated as described in *Materials and Methods* by using the means of the best fit parameters.

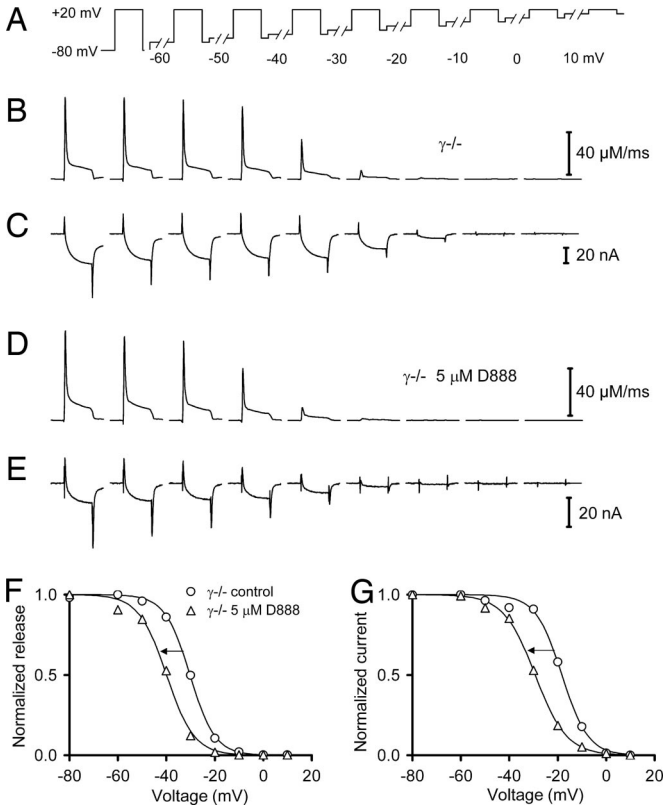

Fig. 3. Effect of D888 on voltage-dependent inactivation. (*A*) Experimental protocol to determine the voltage dependence of inactivation. (*B* and *C*) Calculated Ca^{2+} release fluxes and L-type Ca^{2+} inward currents, respectively, at different voltages in the absence of D888. (*D* and *E*) Release fluxes and inward currents, respectively, in the presence of 5 μM D888. (*F* and *G*) Normalized steady-state voltage dependence of inactivation of peak Ca^{2+} release and Ca^{2+} inward current, respectively, at 0 μm (circles) and 5 μM D888 (triangles). Both fibers were from $\gamma-/-$ mice.

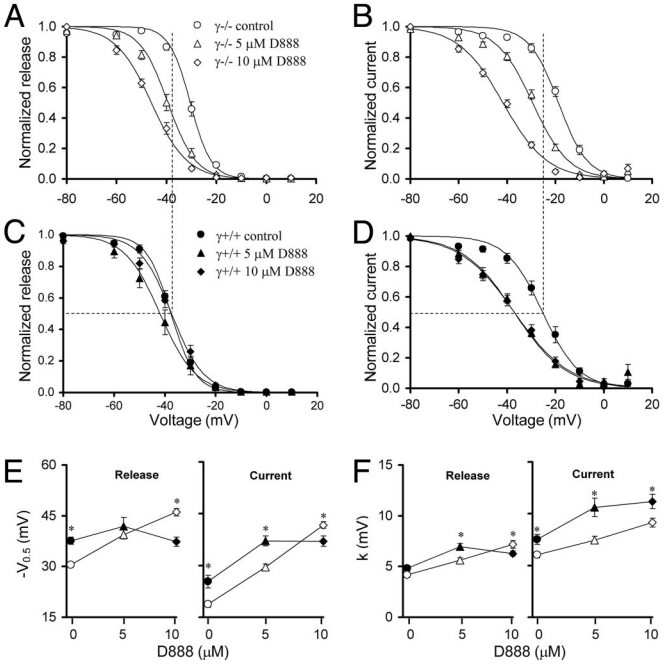

Fig. 4. Changes of steady-state availability caused by D888 in $\gamma-/-$ and $\gamma+/+$ fibers. Mean values of normalized steady-state inactivation at different voltages obtained with the experimental protocol of Fig. 3 for peak Ca^{2+} release flux (*A* and *C*) and L-type Ca^{2+} current (*B* and *D*), respectively. (*A* and *B*) $\gamma-/-$ fibers; (*C* and *D*) $\gamma+/+$ fibers. Numbers of experiments for 0 μm (circles), 5μM (triangles), and 10 μM D888 (diamonds) were 13, 10, and 9 in Fig. 5*A*, 13, 9, and 9 in *B*, 11, 6 and 13 in *C*, and 11, 7, and 13 in *D*, respectively. Note that bars indicating SEM are often smaller than the symbols. (*E* and *F*) Parameters $V_{0.5}$ and *k* of voltage-dependent inactivation and their alteration by D888. Closed symbols, $\gamma+/+$; open symbols, $\gamma-/-$. Asterisks indicate significant differences.

Availability curves obtained in the absence of drug (circles) and in the presence of 5 μM D888 (triangles) and 10 μM D888 (diamonds) are shown. The data for each fiber were fitted by Boltzmann functions and the mean fit parameters of each group of experiments were used to construct the continuous curves. The vertical dashed lines mark the voltages of half-maximal inactivation in drug-free $\gamma+/+$ fibers and highlight the relative differences between $\gamma+/+$ and $\gamma-/-$ fibers in the positions of the curves. Note that the voltages of half-maximal inactivation in 5 μM D888 in the absence of the γ_1-subunit are similar to the values in drug-free $\gamma+/+$ fibers. Thus, 5 μM D888 effectively reverses the right shift caused by the γ_1 elimination.

Fig. 4 *E* and *F* summarize the changes in the Boltzmann fit parameters of the inactivation curves of Fig. 4 *A–D*. Mean values of the parameters $V_{0.5}$ and *k* (which is proportional to the reciprocal of the maximal slope) are plotted versus D888 concentration. The $\gamma-/-$ fibers in the absence of drug (open circles) differ from the $\gamma+/+$ fibers (filled circles) by their more positive $V_{0.5}$ and a slightly smaller *k* value. The differences are almost eliminated in the $\gamma-/-$ fibers by 5 μM D888 (open triangle). $V_{0.5}$ (in millivolts) for L-type current was -25.33 ± 1.81 (11) in drug-free $\gamma+/+$ fibers, compared with -18.77 ± 0.92 (13; $P = 0.0027$) and -29.48 ± 0.87 (9; $P = 0.023$) in drug-free $\gamma-/-$ fibers and $\gamma-/-$ fibers with 5 μM D888, respectively. The $V_{0.5}$ value for Ca^{2+} release was -37.60 ± 1.05 (11; drug-free $\gamma+/+$ fibers), compared with -30.48 ± 0.71 (13; $P = 0.0000093$) and -39.43 ± 1.29 (10; $P = 0.28$), respectively. The corresponding *k* values (in millivolts) were 7.52 ± 0.48, 6.02 ± 0.27 ($P = 0.010$), and 7.43 ± 0.37 ($P = 0.90$) for L-type current and 4.82 ± 0.25, 4.18 ± 0.26 ($P = 0.096$), and 5.6 ± 0.26 ($P = 0.043$) for Ca^{2+} release.

The results of Fig. 4 indicate that (*i*) a concentration of $\approx$5 μM of the PAA drug D888 can compensate for the effect of γ_1 elimination on the voltage dependence of inactivation and that (*ii*) the dependence on D888 concentration is altered by the presence of the γ_1-subunit, consistent with some kind of interaction between the effects of these two modulators of the DHPR.

Both γ_1 and D888 Slow Recovery from Inactivation. We further investigated the time course of recovery from voltage-dependent inactivation by using the pulse protocol of Fig. 5*A*. Pulses of 100-ms duration that depolarized the membrane to +20 mV were applied to test the degree of recovery. An initial test pulse was followed by a 60-s depolarization to +10 mV to cause complete voltage-dependent inactivation. After the long depolarization, the membrane was repolarized to -80 mV. Then, test pulses were applied at different times (indicated in the figure) to resolve the time course of recovery. Fig. 5 *B* and *C* show the calculated Ca^{2+} release flux and the recorded L-type Ca^{2+} current for each of the test pulses in Fig. 5*A*. The time course of the increase in peak release flux and in the amplitude of the L-type current was fitted by single exponential functions. Fig. 5 *D* and *E* show mean values from different experiments of the recovery time constants of Ca^{2+} release and Ca^{2+} current, respectively. In the absence of the drug, the time constants were significantly shorter in $\gamma-/-$ fibers than in $\gamma+/+$ and became larger when D888 was added (5 and 10 μM). Again, 5 μM D888 changed the recovery time constant of $\gamma-/-$ fibers to close to

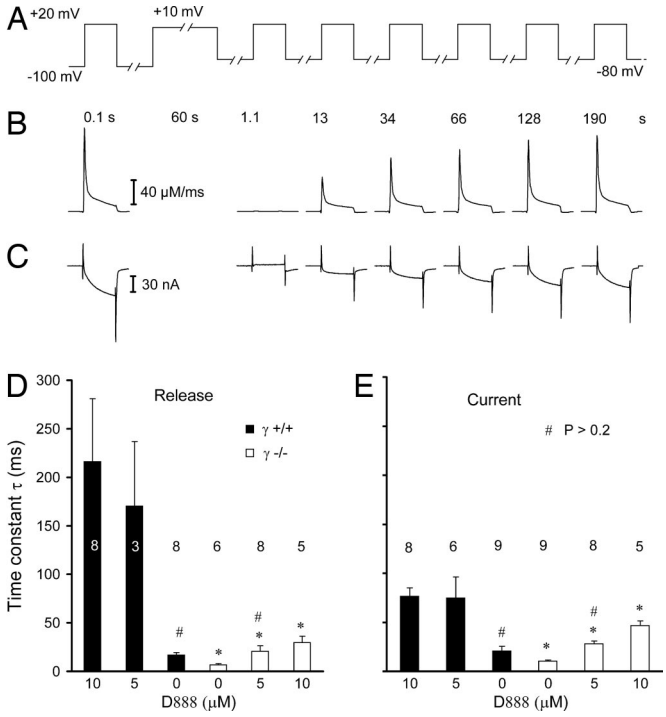

Fig. 5. Alterations of the time course of recovery from depolarization-induced inactivation caused by D888 in $\gamma-/-$ and $\gamma+/+$ fibers. (*A*) Experimental protocol for studying recovery. (*B* and *C*) Representative recordings ($\gamma+/+$) showing recovery at -80 mV of Ca^{2+} release and Ca^{2+} current, respectively. (*D* and *E*) Mean time constants of recovery of peak Ca^{2+} release flux and Ca^{2+} current (end of pulse), respectively, in the absence and in the presence of 5 and 10 μM D888. Asterisks indicate significant differences between $\gamma+/+$ (filled columns) and in $\gamma-/-$ (open columns) for identical drug concentration. The values at 5 μM D888 in $\gamma-/-$ were not significantly different from the controls in $\gamma+/+$ (#, $P = 0.56$ and $P = 0.28$ for release and current, respectively). Error bars indicate SEM. Numbers of experiments are indicated in the figure.

normal values found in $\gamma+/+$ fibers. Remarkably, the slowing of recovery by D888 was substantially stronger in the presence of the γ_1-subunit. These results demonstrate nonadditive effects of the two modulators and provide strong support for an interaction between changes induced by the γ_1-subunit and D888.

γ_1 and Diltiazem Favor Dihydropyridine Binding. A different view on drug modulation of the DHPR results from studying the binding of specific ligands and their allosteric interaction (18, 19). In a further series of experiments, therefore, we used this approach to look for Ca^{2+} antagonist-like effects of the γ_1-subunit. We tested the binding of the dihydropyridine (DHP) Ca^{2+} antagonist isradipine and its modulation by the benzothiazepine drug diltiazem by using microsomal membrane proteins from $\gamma-/-$ and $\gamma+/+$ mice. Fig. 6*A* shows that specific high-affinity binding of isradipine was reduced in $\gamma-/-$ muscle. This reduction depends on temperature and is not observed at 4°C (20). On average, B_{max} showed a 58% decrease compared with $\gamma+/+$, but binding recovered to more than normal levels after adding 10 μM diltiazem (Fig. 6*B*, see legend for details). Because the allosteric effect of diltiazem on DHP-binding is also temperature-dependent, we performed the experiments at different temperatures. Fig. 6 *C* and *D* show the dependence of isradipine binding on diltiazem concentration at 37 and 21°C. The graphs demonstrate that the reduced binding in the absence of the γ_1-subunit could in both cases be restored to $\gamma+/+$ levels by appropriate diltiazem concentrations. This is further evidence for a Ca^{2+} antagonist-like effect of the γ_1-subunit and further demonstration that a Ca^{2+} antagonistic drug can compensate for the effect of eliminating the γ_1-subunit.

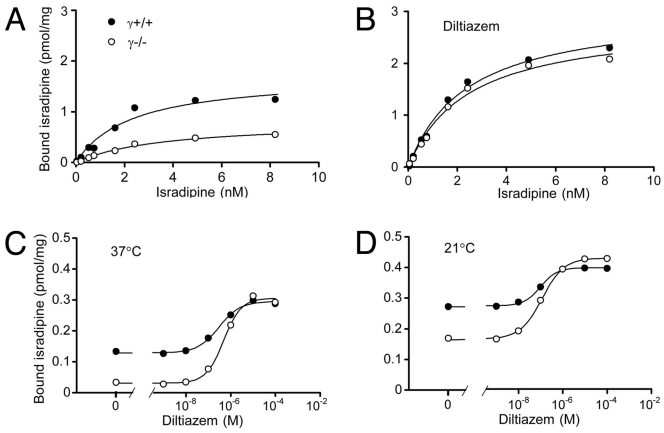

Fig. 6. Interaction of γ_1-subunit with allosteric modulation of isradipine binding by diltiazem. (*A* and *B*) Equilibrium isotherms of [^{3}H]isradipine binding to skeletal muscle microsomes from $\gamma+/+$ (filled symbols) and $\gamma-/-$ animals (open symbols) in the absence (*A*) and presence (*B*) of D-*cis*-diltiazem (10 μM) at 37°C. Least-squares fitting of canonical binding curves to the data resulted in the following values for B_{max} (pmol/mg). Control, $\gamma+/+$: 1.71 ± 0.12 (4); control, $\gamma-/-$: 0.72 ± 0.09 (4); diltiazem, $\gamma+/+$: 3.28 ± 0.15 (4); diltiazem, $\gamma-/-$: 2.97 ± 0.25 (4). Except for the difference between the latter two values, all pairwise differences were highly significant ($P < 0.001$). K_d values (nM) were as follows: 2.08 ± 0.37, 2.93 ± 0.79, 2.25 ± 0.26, and 2.54 ± 0.50. They showed no significant differences. (*C* and *D*) Effect of increasing concentrations of D-*cis*-diltiazem on the amount of [^{3}H]isradipine (0.5 nM) bound to microsomes from $\gamma+/+$ (filled symbols) and $\gamma-/-$ animals (open symbols) at 37°C (*C*) and 21°C (*D*). The figure shows representative data from individual experiments that were repeated at least twice.

Discussion

In the present study we explored the impact of the γ_1-subunit of the DHPR on Ca^{2+} antagonist action by using wild-type and γ_1-deficient mice. We found that D888, a phenylalkylamine drug, (*i*) did not affect the voltage dependence of activation but enhanced steady-state inactivation and slowed down recovery from inactivation, (*ii*) compensated for the effect of γ_1 deficiency, and (*iii*) was substantially altered in its effect by the presence of the γ_1-subunit. Finally, studying drug binding to the DHPR, we showed that a structurally unrelated Ca^{2+} antagonist (the benzothiazepine diltiazem) likewise compensated for the effect of γ_1 elimination. Together, these results indicate that γ_1 can be regarded as an endogenous Ca^{2+} antagonist.

Comparison with Previous Studies on PAA Action in Skeletal Muscle Excitation-Contraction (EC) Coupling. Alterations of the voltage dependence of inactivation of EC coupling induced by PAA drugs in skeletal muscle were discovered by force recordings from voltage-clamped frog muscle fibers (5). The changes have been explained by different variants of the voltage-modulated receptor concept. In analogy to the effects of local anesthetics on Na^+ channels (21), the proposed models suggest preferential binding of PAA drugs to inactivated states of the voltage sensor (6, 7, 22). For frog fibers, Erdmann and Lüttgau (6) reported a change of $V_{0.5}$ of the voltage dependence of availability by -46 mV induced by 5 μM (−)D888. In the mouse fibers studied here, the same concentration caused a maximal shift by 10.5 mV (Fig. 4). Much of the difference is likely due to the experimental temperature (10°C in the frog experiments vs. 20–22°C in our case), because low temperatures have been shown to augment paralysis in frog fibers (4, 23). Low temperatures also favored binding of D888 to the purified rabbit DHPR (24). A further reason for the stronger D888 effect in the frog experiments may be the fact that availability at different potentials was studied by determining the degree of recovery from a preceding complete

inactivation. Because D888 significantly slows recovery kinetics, a true steady state may not have been attained in the observation interval, causing an overestimation of the left shift in the voltage dependence.

γ_1-Subunit Interference with Drug Effects. Ursu *et al.* (12) established that in muscle fibers deficient in the DHPR γ-subunit the voltage dependence of availability was shifted to more positive potentials for both Ca^{2+} current and Ca^{2+} release, whereas the voltage dependence of activation remained unchanged. Considering the PAA effects on EC coupling, these findings indicate a PAA-like effect of the γ_1-subunit. Accordingly, we could show that D888 fully reversed the consequences of the subunit knockout: $\approx$5 μM D888 (when applied to $\gamma-/-$ fibers) was equivalent to the presence of γ_1, essentially restoring normal EC coupling and L-type channel function. It is interesting to note that Ca^{2+} release and L-type Ca^{2+} current were affected in a very similar way. This observation adds to evidence (see ref. 25) in support of the hypothesis that there are not two different pools of DHPRs for the voltage control of Ca^{2+} release and Ca^{2+} entry, respectively, but that an individual DHPR can perform both functions.

Furthermore, comparing the effect of D888 in $\gamma+/+$ and $\gamma-/-$ fibers, we noticed clear differences. Not only did the drug affect the voltage dependence of availability differently in the two types of fibers, but also the slowing of recovery caused by D888 was substantially augmented in the presence of the γ_1-subunit. This reveals a combined but nonadditive effect of the drug and the auxiliary polypeptide. It is well known that members of the chemically heterogeneous groups of Ca^{2+} channel agents, dihydropyridines, benzothiazepines and phenylalkylamines, and metal ions show characteristic noncompetitive interactions when binding to the α_1-subunit of the DHPR (18, 19, 26). For instance, diltiazem (a benzothiazepine Ca^{2+} antagonist) favors the binding of DHPs in skeletal muscle (27–29). Performing similar investigations, our aim was to back up the conclusion that the auxiliary subunit γ_1 is an endogenous Ca^{2+} antagonist by using an independent experimental setting (i.e., binding studies) and drugs different from D888 (i.e., the DHP isradipine and D-*cis*-diltiazem). We showed that an effect on isradipine binding similar to the one found for diltiazem can be attributed to the γ_1-subunit and that diltiazem compensates for the effect of γ_1 knockout. Like diltiazem, γ_1 accomplished recovery of the intact drug binding domain of the DHPR, preferentially by increasing B_{max} rather than by affecting binding affinities (Fig. 6). Also, the PAA drug D600 has been reported to stimulate high-affinity DHP binding, thus mimicking the effect of γ_1 in a heterologous expression system (30, 31). Therefore, the results on drug binding are consistent with our functional data indicating a cross-influence between γ_1 and the drug binding sites.

Several amino acid residues in segments IIIS6, IVS6, and the S5-S6 linkers of domains III and IV contribute to Ca^{2+} antagonist binding in L-type Ca^{2+} channels (reviewed in ref. 26). The available data suggested a drug binding pocket near the pore region (32) and led to the proposal of a "domain interface model" in which the drugs affect gating by binding to the contact region between the homologous repeats III and IV of the α_1-subunit (19, 33). As for the common Ca^{2+} antagonistic drugs, γ_1 has been shown to interact directly with α_{1S} (34). Little is known about the structural determinants of the interaction, however, except that the first (N-terminal) half of γ_1 is required for association (34). Given the very similar effect of γ_1 and Ca^{2+} antagonistic drugs, the C-terminal repeats of the α_1-subunit that form the drug binding sites may also contain the receptor for γ_1-subunit binding. This receptor, once occupied, seems to foster slow inactivation like a PAA drug. For steric reasons, it may seem unlikely that γ_1 reaches the putative drug binding pocket near the selectivity filter. However, it is conceivable that a domain interface effect may also arise by binding of the polypeptide to the outer region of the III–IV interface.

It has been suggested (for a summary, see ref. 35) that the L-type channel drugs might mimic effects of endogenous modulators (possibly peptides) in analogy to morphine and its derivatives acting on receptors for intrinsic endorphins and enkephalins. We suppose that γ_1 is such an endogenous ligand. Like Ca^{2+} antagonists, γ_1 might modulate voltage-dependent inactivation by association to and dissociation from the α_1-polypeptide. Shifting back and forward the voltage dependence of inactivation, γ_1 has the potential to act as a modulator of EC coupling and consequently contractile force. Intensive activation of skeletal muscle leads to substantial K^+ release from the fibers (36). The ensuing accumulation of K^+ ions in the extracellular space and in the narrow transverse tubules, possibly in conjunction with local fiber damage, leads to membrane depolarization. When strong enough, steady depolarization would cause maintained Ca^{2+} release and consequently involuntary muscle contractures. The slow inactivation process of the DHPR can be envisaged as a mechanism to counteract such effects, but it leaves a window of voltages in which steady activation is possible (12, 37). Agents with the functional characteristics of Ca^{2+} antagonists will narrow this window. The purpose of the γ_1-subunit as an endogenous Ca^{2+} antagonist can therefore be regarded as protection against uncontrolled Ca^{2+} release and Ca^{2+} entry under certain highly fatiguing conditions that would lead to partial membrane depolarization.

Materials and Methods

Preparation. Male littermates of $\gamma+/+$ (between 45 and 70 weeks of age) and $\gamma-/-$ mice (50–77 weeks of age) carrying the 129SVJ genetic background (see ref. 20) were used for the electrophysiological experiments. Mice were killed by rapid exposure to CO_2 followed by cervical dislocation. Procedures were approved by the local animal care committee. Fibers of the interosseus muscles of the hind legs were enzymatically dissociated by using a Krebs–Ringer solution containing 2 mg/ml collagenase as described in ref. 13. Microsomal membrane proteins were prepared from hind leg skeletal muscle of adult mice at 4°C in the presence of 5 mM EGTA. All buffers used in binding experiments contained a protease-inhibitor mix as described in ref. 20.

Experimental Solutions for Electrophysiological Experiments. External bathing solution for voltage-clamp experiments contained 130 mM tetraethylammonium-OH, 130 mM HCH_3SO_3, 2 mM $MgCl_2$, 10 mM $CaCl_2$, 5 mM 4-aminopyridine, 10 mM Hepes, 0.001 mM Tetrodotoxin, 5 mM glucose, and 0.05 mM *N*-benzyl-*p*-toluene sulfonamide (pH 7.4). (−)D888 (desmethoxyverapamil, devapamil) was added from a 10 mM stock. Pipette solution for intracellular perfusion contained 145 mM CsOH, 110 mM aspartic acid, 0.75 mM Na_2ATP, MgATP (5.16 mM Mg^{2+}, 4.25 mM ATP), 1.5 mM $CaCl_2$, 10 mM Hepes, 15 mM EGTA, 0.2 mM fura-2, and 5 mM $Na_2creatinePO_4$ (pH 7.2).

Voltage Clamping and Data Analysis. The experiments were performed at room temperature (20–22°C). The experimental chamber was mounted on an inverted fluorescence microscope (Axiovert 135 TV, Zeiss, Thornwood, NY). Fibers bathed in external solution were imaged with a ×40/0.75W objective (Zeiss) after attaching to the glass coverslip in the bottom of the chamber. They were voltage-clamped in a two-electrode configuration by use of an Axoclamp 2B amplifier (Axon Instruments, Union City, CA) as described in refs. 12 and 13. Fibers were perfused by the fura-2-containing solution in the current-passing electrode. The general holding potential during loading with the pipette solution, and throughout the experiment, was −80 mV. Between experimental protocols that included long-lasting depolarizations, the fiber membrane was hyperpolarized to −100

mV to speed up recovery. Global Ca^{2+} signals (fura-2 fluorescence) and L-type Ca^{2+} currents were simultaneously recorded at 2-kHz sampling frequency. For constructing current–voltage relations, the measured values during the last 10 ms of step depolarizations (100 ms) were averaged and plotted vs. step voltage. Ratiometric Ca^{2+} transients were analyzed with a removal model fit approach as originally described by Melzer *et al.* (38) to calculate the flux of Ca^{2+} from the SR (see refs. 13 and 39). The estimates of Ca^{2+} release flux and of the SR-luminal Ca^{2+} concentrations are proportional to the assumed intracellular EGTA concentration (39). For the removal analysis we used the pipette concentrations of EGTA and fura-2 and subsequently scaled down the resulting flux amplitudes and SR-luminal Ca^{2+} concentrations by a factor of 0.4 to account for mean fractional loading of the cell at the time of recording (12). The voltage-activated Ca^{2+} permeability of the SR (in % ms^{-1}) was calculated according to Gonzalez and Ríos (17) under the assumption that the slow decline in the plateau phase of the Ca^{2+} release flux results exclusively from SR depletion. The voltage dependence of activation and inactivation was described by canonical Boltzmann functions with voltage at half-maximum $V_{0.5}$ and steepness parameter k, except for the activation of Ca^{2+} release and permeability in which a linear term was included to account for the behavior at large depolarizations (13).

Binding Experiments. The binding of the DHP (+)[^{3}H]isradipine ((+)-[*methyl*-^{3}H]PN200-110, 69.0 Ci/mmol; Amersham GE Healthcare, Princeton, NJ) was determined in 0.25 ml of 50 mM Tris·Cl, pH 7.4/5 mM EGTA, containing 45–75 μg of microsomes (microsomal protein) in the absence or presence of 1 μM (±)-isradipine. Seventy to 95% of total binding was specific. D-*cis*-diltiazem was added as indicated. Reactions were stopped after 60 min (21°C) and 30 min (37°C), respectively, by addition of 3 ml of ice-cold 8.5% (mass/volume) polyethyleneglycol 6000/100 mM Hepes, pH 7.4, as described in ref. 20. Single binding values were determined in triplicate and experiments were repeated at least twice by using different skeletal muscle membrane protein preparations.

Statistics. Averaged data are presented and plotted as means ± SEM (n = number of experiments). To test for significant differences of mean values, we used Student's two-sided t test for two independent populations ($P < 0.05$).

We thank Dr. R. P. Schuhmeier for stimulating discussions and for developing the analysis software; Dr. F. Lehmann-Horn, the director of the Institute of Applied Physiology, for support; and C. Störger, K. Fuchs, A. Riecker, and E. Schoch for expert technical help. This work was supported by Deutsche Forschungsgemeinschaft (DFG) Grants ME-713/10-3 and ME-713/18-1 (to W.M.) and SFB 530, A1 (to V.F.). Z.A. was funded in part by research-training Grant HPRN-CT-2002-00331 from the European Commission (to W.M.).

1. Flaim SF, Zelis R (1982) *Calcium Blockers: Mechanisms of Action and Clinical Applications* (Urban & Schwarzenberg, Baltimore).
2. Fleckenstein A (1983) *Calcium Antagonism in Heart and Smooth Muscle* (Wiley, New York).
3. Melzer W, Herrmann-Frank A, Lüttgau HC (1995) *Biochim Biophys Acta* 1241:59–116.
4. Eisenberg RS, McCarthy RT, Milton RL (1983) *J Physiol (London)* 341:495–505.
5. Berwe D, Gottschalk G, Lüttgau HC (1987) *J Physiol (London)* 385:693–707.
6. Erdmann R, Lüttgau HC (1989) *J Physiol (London)* 413:521–541.
7. Pizarro G, Brum G, Fill M, Fitts R, Rodriguez M, Uribe I, Rios E (1988) in *The Calcium Channel, Structure, Function, and Implications*, eds Morad M, Nayler W, Kazda S, Schramm M (Springer, Berlin), pp 138–158.
8. Feldmeyer D, Melzer W, Pohl B (1990) *J Physiol (London)* 421:343–362.
9. Hanlon MR, Wallace BA (2002) *Biochemistry* 41:2886–2894.
10. Arikkath J, Campbell KP (2003) *Curr Opin Neurobiol* 13:298–307.
11. Flucher BE, Obermair GJ, Tuluc P, Schredelseker J, Kern G, Grabner M (2005) *J Muscle Res Cell Motil* 26:1–6.
12. Ursu D, Schuhmeier RP, Freichel M, Flockerzi V, Melzer W (2004) *J Gen Physiol* 124:605–618.
13. Ursu D, Schuhmeier RP, Melzer W (2005) *J Physiol (London)* 562:347–365.
14. Melzer W, Ríos E, Schneider MF (1987) *Biophys J* 51:849–863.
15. Timmer J, Müller T, Melzer W (1998) *Biophys J* 74:1694–1707.
16. Schneider MF, Simon BJ, Szücs G (1987) *J Physiol (London)* 392:167–192.
17. Gonzalez A, Ríos E (1993) *J Gen Physiol* 102:373–421.
18. Hockerman GH, Peterson BZ, Johnson BD, Catterall WA (1997) *Annu Rev Pharmacol Toxicol* 37:361–396.
19. Striessnig J, Grabner M, Mitterdorfer J, Hering S, Sinnegger MJ, Glossmann H (1998) *Trends Pharmacol Sci* 19:108–115.
20. Freise D, Held B, Wissenbach U, Pfeifer A, Trost C, Himmerkus N, Schweig U, Freichel M, Biel M, Hofmann F, *et al.* (2000) *J Biol Chem* 275:14476–14481.
21. Hille B (1977) *J Gen Physiol* 69:497–515.
22. Ríos E, Pizarro G (1991) *Physiol Rev* 71:849–908.
23. Siebler M, Schmidt H (1987) *Pflügers Arch* 410:75–82.
24. Schneider T, Regulla S, Hofmann F (1991) *Eur J Biochem* 200:245–253.
25. Lamb GD (1992) *J Muscle Res Cell Motil* 13:394–405.
26. Mitterdorfer J, Grabner M, Kraus RL, Hering S, Prinz H, Glossmann H, Striessnig J (1998) *J Bionenerg Biomembr* 30:319–334.
27. Brauns T, Prinz H, Kimball SD, Haugland RP, Striessnig J, Glossmann H (1997) *Biochemistry* 36:3625–3631.
28. Flockerzi V, Oeken HJ, Hofmann F (1986) *Eur J Biochem* 161:217–224.
29. Glossmann H, Linn T, Rombusch M, Ferry DR (1983) *FEBS Lett* 160:226–232.
30. Suh-Kim H, Wei X, Birnbaumer L (1996) *Mol Pharmacol* 50:1330–1337.
31. Suh-Kim H, Wei X, Klos A, Pan S, Ruth P, Flockerzi V, Hofmann F, Perez-Reyes E, Birnbaumer L (1996) *Recept Channels* 4:217–225.
32. Beyl S, Timin EN, Hohaus A, Stary A, Kudrnac M, Guy RH, Hering S (2007) *J Biol Chem* 282:3864–3870.
33. Catterall WA, Striessnig J (1992) *Trends Pharmacol Sci* 13:256–262.
34. Arikkath J, Chen CC, Ahern C, Allamand V, Flanagan JD, Coronado R, Gregg RG, Campbell KP (2003) *J Biol Chem* 278:1212–1219.
35. Triggle DJ (1988) in *The Calcium Channel: Structure, Function and Implications*, eds Morad M, Nayler W, Kazda S, Schramm M (Springer, Berlin), pp 549–563.
36. Sejersted OM, Sjogaard G (2000) *Physiol Rev* 80:1411–1481.
37. Chua M, Dulhunty AF (1988) *J Gen Physiol* 91:737–757.
38. Melzer W, Ríos E, Schneider MF (1986) *J Physiol (London)* 372:261–292.
39. Schuhmeier RP, Melzer W (2004) *J Gen Physiol* 123:33–51.